universe

MDPI

Article

Spectro-Polarimetric Properties of CHIME FRB Sources

Dengke Zhou [1], Yi Feng [1,2,*], Jiaying Xu [1], Chenyuan Xu [1] and Jianhua Fang [1]

[1] Research Center for Computational Earth and Space Science, Zhejiang Laboratory, Hangzhou 311100, China; zdk@zhejianglab.com (D.Z.); xujy@zhejianglab.com (J.X.); xuchenyuan@zhejianglab.org (C.X.); fangjh@zhejianglab.com (J.F.)

[2] Institute for Astronomy, School of Physics, Zhejiang University, Hangzhou 310027, China

* Correspondence: yifeng@zhejianglab.org

Abstract

Fast radio bursts (FRBs) are enigmatic millisecond-duration radio transients whose polarization properties offer crucial insights into their origins and environments. In particular, low-frequency depolarization—quantified by the parameter $\sigma_{\rm RM}$—probes the complex magneto-ionic medium surrounding the progenitor, and has been observed across a population of repeating FRBs. We present a systematic spectro-polarimetric analysis of repeating and non-repeating FRBs using observations from the Canadian Hydrogen Intensity Mapping Experiment (CHIME). For 28 repeating FRBs, we measure $\sigma_{\rm RM}$, expanding the known sample from 14 to 36 sources (an increase by a factor of 2.6). The kernel density estimate (KDE) of the repeating population peaks at 1.3 rad m^{-2}, with approximately 70% of the sources showing $\sigma_{\rm RM} \gtrsim 1$ rad m^{-2}, implying that most reside in complex magneto-ionic environments. For 70 non-repeating FRBs, we investigate four spectro-polarimetric models; no source exhibits significant depolarization with $\sigma_{\rm RM} \gtrsim 5$ rad m^{-2}. Roughly half of the non-repeaters are consistent with a constant linear polarization fraction across frequency. We caution, however, that these results may be affected by the limited frequency coverage of CHIME. Future ultra-wideband polarimetry, spanning widely separated frequencies, will overcome current observational biases, enable precise $\sigma_{\rm RM}$ measurements, and substantially deepen our understanding of FRB environments.

Keywords: fast radio bursts; polarization; spectral depolarization; CHIME

1. Introduction

Fast radio bursts (FRBs) are enigmatic millisecond-duration extragalactic radio transients. Since the discovery of the first FRB in 2007 [1], the known FRB population has grown rapidly, driven by the increasing sensitivity and survey capabilities of modern radio telescopes. Repeating FRBs are FRBs that originate from sources that emit multiple bursts over time. According to current statistics compiled in the Blinkverse database[1] [2], more than 4000 FRBs have been publicly reported to date; repeating FRBs constitute only a small fraction (∼2.5%) of the total known population, while the majority (∼97.5%) have been detected as one-off events. Despite these advances, including precise localization and host-galaxy identification for a growing number of sources [3], the physical origin, emission mechanism, and environmental properties of FRBs remain largely unresolved [4].

Polarization provides one of the most powerful diagnostics for understanding the physical nature and local environments of FRBs. Precise measurements of polarization can probe the magneto-ionic medium surrounding the source and provide important insights into the underlying radiation mechanism and propagation effects along the line of sight.

Check for updates

Academic Editors: Hai-Nan Lin and Yu Sang

Received: 28 June 2026
Revised: 23 August 2026
Accepted: 25 August 2026
Published: 26 August 2026

Copyright: © 2026 by the authors. Licensee MDPI, Basel, Switzerland. This article is an open access article distributed under the terms and conditions of the Creative Commons Attribution (CC BY) license.

The linear polarization position angle rotates as the radio wave propagates through magnetized plasma, and the magnitude of this effect is quantified by the rotation measure (RM), which reflects the integrated electron density and magnetic field along the line of sight. The RM of repeating FRBs may vary depending on their environments [5]. Observationally, a significant proportion of repeating FRBs show RM variations [6]. The RM of FRB 20121102A dropped substantially over time [7,8]. RM reversals have been observed in sources including FRB 20190520B, FRB 20190117A, and FRB 20220529A [6,9–11]. An RM jump was also observed in FRB 20220529A [11]. These observations suggest that these repeating FRBs reside in dynamic magneto-ionic environments, possibly including expanding supernova remnants, pulsar wind nebulae, and massive binary systems [5,12–16].

Complex environments may leave imprints on the spectro-polarimetric properties of FRBs. The linear polarization fraction may become frequency-dependent, with the magnitude of this dependence characterized by the RM scatter $\sigma_{\rm RM}$ [17]. Using observations from several telescopes covering 115 MHz to 4.6 GHz, Feng et al. [18] reported depolarization behavior in repeating FRBs: the linear polarization fraction decreases steadily toward lower frequencies, quantified by $\sigma_{\rm RM}$ values between 0.12 and 218 rad m^{-2}, attributed to multipath scattering in turbulent magneto-ionic environments. This depolarization behavior not only probes the intervening magneto-ionic medium and constrains possible progenitors and emission mechanisms, but may also point to a distinctive environmental link: the two FRBs with the largest $\sigma_{\rm RM}$, namely FRB 20121102A (30.9 ± 0.4 rad m^{-2}) and FRB 20190520B (218 ± 10.2 rad m^{-2}), are both known to be associated with persistent radio counterparts [18–20]. The linear regression between log |RM| and log $\sigma_{\rm RM}$ for the repeating FRB sample yields a slope of 0.62 ± 0.30 [18].

Using the Australian Square Kilometre Array Pathfinder (ASKAP) sample, a search for depolarization was conducted in 17 apparently non-repeating FRBs [21,22]. Only FRB 20230526A shows clear frequency-dependent depolarization, with its linear polarization fraction dropping from ∼60% at high frequencies (1440 MHz) to ∼20% at low frequencies (1110 MHz). For the other non-repeating bursts, upper limits on $\sigma_{\rm RM}$ were derived under two scenarios: assuming 100% intrinsic linear polarization (Burn model, denoted as $\sigma_{\rm RM}$) and allowing the intrinsic polarization to be free (modified Burn model, denoted as $\sigma'_{\rm RM}$, which yields more conservative upper limits) [21,22]. When these upper limits are compared with the log |RM|–log $\sigma_{\rm RM}$ relation obtained by Feng et al. [18], they are found to be consistent only if the actual $\sigma_{\rm RM}$ values are roughly two orders of magnitude smaller than $\sigma'_{\rm RM}$ [21,22].

In this paper, we use the published polarimetric data of repeating and non-repeating FRBs from the Canadian Hydrogen Intensity Mapping Experiment (CHIME) [23,24] to measure $\sigma_{\rm RM}$ for 28 repeating FRBs and to compare four different spectro-polarimetric models against 70 non-repeating FRBs. The paper is structured as follows: Section 2 describes our method; Section 3 presents the main results; and Section 4 summarizes our key conclusions.

2. Method

In this work, we analyze two complementary FRB samples: repeating FRBs from CHIME/FRB [24,25] and non-repeating FRBs from the first CHIME/FRB baseband catalog [23].

For repeating FRBs, we adopt the polarization measurements from Ng+2025 [24], which include 28 repeating sources. Ng+2025 provides a comprehensive study of RM temporal variability and polarization for 28 repeaters, with a distinct emphasis from this work. Critically, Ng+2025 does not examine the $\sigma_{\rm RM}$ associated with Burn-type depolarization, nor does it perform model comparisons on the frequency dependence of L/I. Our $\sigma_{\rm RM}$

measurements for repeaters therefore comprise a new and complementary analysis using the published measurements from Ng+2025, rather than a reinterpretation of their results. In Ng+2025, the baseband data were localized and beamformed to each repeater's sky position, coherently de-dispersed at the structure-optimized DM, and processed through the standard CHIME/FRB polarization pipeline [26] to obtain Stokes I, Q, U, V dynamic spectra. The linear polarization fraction L/I for each burst was then calculated by integrating $L = \sqrt{Q^2 + U^2}$ over the burst profile.

For non-repeating FRBs, we adopt the sample from Ref. [23], which consists of 89 polarized bursts from the first CHIME/FRB baseband catalog. We first retain only bursts with total signal-to-noise ratio (S/N) ≥ 6, following the S/N ≥ 6 threshold adopted by Ng et al. [24] for linear polarization detection. This selection reduces the sample to 70 non-repeating FRBs. For each burst, we use the RM derived from QU-fitting by the CHIME/FRB polarization pipeline [26] to apply Faraday de-rotation to the Stokes Q and U spectra. For non-repeating FRBs, these QU-fitting RM values are taken from the published catalog of Pandhi et al. [23] (denoted $\mathrm{RM_{QU}}$, listed in Supplementary Tables S2 and S3). After de-rotation, we integrate the derotated Stokes spectra over the burst envelope and divide the band into sub-bands using an adaptive binning scheme: starting from a minimum interval of 5 MHz, each sub-band is iteratively widened in 5 MHz steps until the total intensity S/N in that sub-band exceeds 5. This allows us to extract the linear polarization fraction L/I as a function of λ^2 with finer resolution where the signal is strong while maintaining sufficient S/N in each sub-band.

For each repeating FRB, we compute σ_{RM} from the Burn model [17], which describes depolarization as

$$P_{\mathrm{lin}}(\lambda^2) = \exp(-2\sigma_{\mathrm{RM}}^2\lambda^4), \tag{1}$$

where P_{lin} is the linear polarization fraction at wavelength λ. For each burst, σ_{RM} is obtained by inverting Equation (1) using the published L/I measurement. In the absence of any published estimates of systematic uncertainties in CHIME polarization data, we add a systematic uncertainty of 0.05 on L/I in quadrature with the statistical errors to properly assess the uncertainties in σ_{RM}. This adopted systematic uncertainty is an order of magnitude larger than the value reported for the Five-hundred-meter Aperture Spherical radio Telescope (FAST) [27]. For FRBs with multiple bursts, we take the minimum σ_{RM} among all bursts as the representative value for the source.

For non-repeating FRBs, we compare four spectro-polarimetric models to identify the best-fit description of the spectro-polarimetric behavior: (1) the Burn model, (2) a modified Burn model allowing for non-unity high-frequency polarization, (3) a constant spectro-polarimetric model, and (4) an oscillation model [28] that captures coherent oscillations in polarization fraction. Motivated by Faraday conversion [28,29] or instrumental effects [26], we introduce the oscillation model. The oscillation model is first fit jointly to the linear and circular polarization fractions, sharing a common angular frequency ω between the two polarization components. The best-fit linear-polarization parameters are then extracted from the joint posterior samples, and the marginal likelihood for the linear polarization data alone is computed via Monte Carlo integration: for each posterior sample from the joint fit, the linear-polarization likelihood is evaluated, and the marginal likelihood is obtained as the average of these likelihood values over the samples. This enables a fair Bayesian comparison with the other three models, which are fit directly to the linear polarization data via nested sampling. All four models are compared on the same linear polarization data using Bayesian evidence, with $\Delta \log_{10} E \geq 10$ adopted as the uniform threshold for strong evidence in favor of one model over another [21,30]. In addition, we compute posterior predictive check (PPC) p-values as a quantitative goodness-of-fit diagnostic. For bursts where the oscillation model is preferred by Bayesian evidence, we further require that the

linear polarization oscillation amplitude be detected at high significance ($A/\sigma_A > 7$) in the joint fit, together with visual inspection of the fitted oscillation pattern, ensuring that the oscillatory structure is genuinely present rather than arising from noise fluctuations.

1. Oscillation model:
$$P_{\rm lin}(\lambda^2) = c + k\lambda^2 + A\sin(\omega\lambda^2 + \phi_0), \quad (2)$$
where A is the amplitude of sinusoidal variation, ω the angular frequency (shared with circular polarization), ϕ_0 the initial phase, k the linear slope, and c the baseline polarization. This model captures coherent oscillations in polarization fraction induced by propagation effects in magnetized plasma. The oscillation phases of linear and circular polarizations are roughly π radians out of phase.
2. Constant model:
$$P_{\rm lin}(\lambda^2) = P_0, \quad (3)$$
where P_0 is the constant linear polarization fraction, which represents wavelength-independent linear polarization, indicative of negligible Faraday depolarization within the observational band.
3. Burn model (Equation (1)), describing depolarization dominated by random RM variations.
4. Modified Burn model:
$$P_{\rm lin}(\lambda^2) = P_0 \exp(-2{\sigma'_{\rm RM}}^2\lambda^4), \quad (4)$$
where P_0 is the intrinsic polarization and $\sigma'_{\rm RM}$ characterizes depolarization due to RM dispersion. This model allows the intrinsic polarization fraction (at infinite frequency) to deviate from 100%.

The model fitting and Bayesian evidence calculations described above are performed with custom Python (v3.11.14) scripts based on the `dynesty` (v3.0.0) package for nested sampling. To better reflect the true scatter, we rescale the uncertainties on $\sigma_{\rm RM}$ and $\sigma'_{\rm RM}$ by a factor of $\sqrt{\chi^2_\nu}$ when performing the parameter estimation, where $\chi^2_\nu = \chi^2/(N-d)$ is the reduced chi-squared statistic of the best-fit model, with N data points and d free parameters.

3. Results

3.1. Repeating FRBs

Figure 1 shows the kernel density estimates (KDE) of the linear polarization fraction for three repeating FRBs (FRBs 20240114A, 20220912A, and 20201124A; red, orange, and blue curves, respectively), based on measurements from Ref. [31–33] with FAST and Robert C. Byrd Green Bank Telescope (GBT), together with the KDE for our CHIME repeater sample (28 sources; black curve) [24]. The colored curves show a sharp peak at high linear polarization fractions ($\gtrsim$80%–100%), with median values of 95.5%, 96.0%, and 93.6% for FRBs 20201124A, 20220912A, and 20240114A, respectively [31–33], all falling within this high range. By contrast, the black KDE for the CHIME sample is significantly broader and extends to much lower polarization fractions, providing clear evidence that the CHIME repeater population experiences depolarization.

Using the method described in Section 2, we measure $\sigma_{\rm RM}$ for the 28 repeating FRBs. The resulting $\sigma_{\rm RM}$ values are summarized in Supplementary Table S1 (the corresponding RM values are from the CHIME/FRB polarization pipeline, as reported by Ng et al. [24]), and the distribution of $\sigma_{\rm RM}$ is shown in Figure 2. Previous studies reported $\sigma_{\rm RM}$ measurements for 14 repeaters [10,18,34]. Our sample expands this to 36 repeaters (adding 22 new ones), representing an increase by a factor of 2.6. Approximately 70% of the sources exhibit $\sigma_{\rm RM} \gtrsim 1$ rad m^{-2}, implying that they reside in complex magneto-ionic environments.

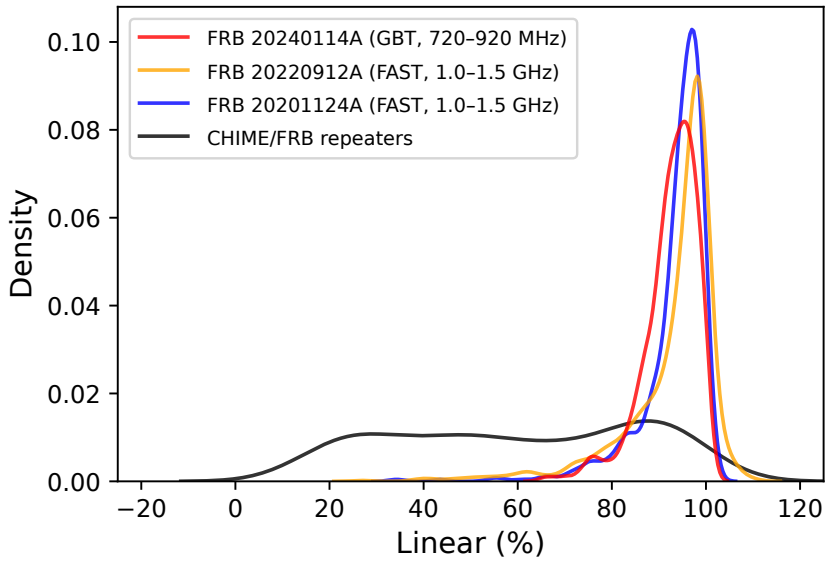


Figure 1. Linear polarization distributions of several repeating FRBs and the CHIME/FRB repeater sample. The figure presents the KDE of the linear polarization degree for three repeating FRBs (red, orange, and blue curves), together with that of the CHIME/FRB repeater sample (black curve) [24]. The KDE tails extending beyond the physical bounds (0% and 100%) are artifacts of the kernel smoothing and do not represent real physical probability.

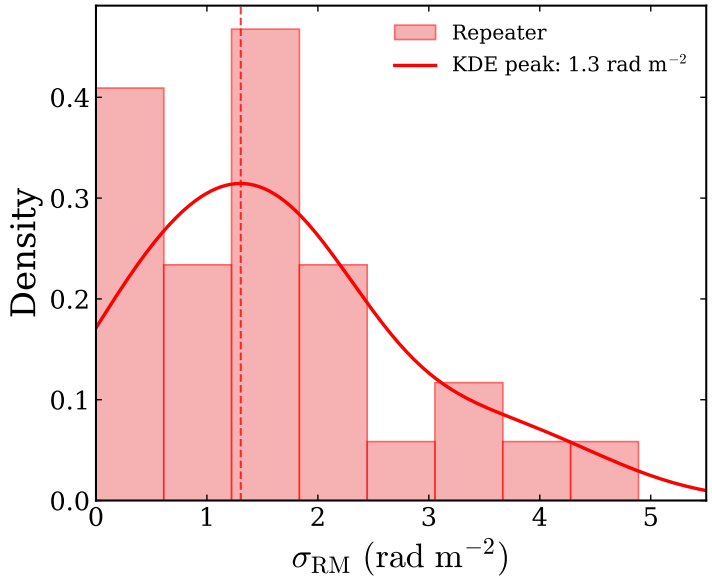


Figure 2. Distribution of $\sigma_{\rm RM}$ for the 28 repeating FRBs. The histogram and KDE curve show the normalized density. The red dashed line marks the KDE peak at 1.3 rad m^{-2}.

The largest $\sigma_{\rm RM}$ measured in our sample is $\sim$5 rad m^{-2}, and we find no source with $\sigma_{\rm RM} > 10$ rad m^{-2}. We interpret this absence as a consequence of selection bias. For instance, a $\sigma_{\rm RM}$ of 7.6 rad m^{-2} would already suppress the linear polarization fraction to $\sim$10% at 800 MHz, the high-frequency end of the CHIME band. Given that most bursts in our sample have total S/N below 100, and that we typically require a linear polarization S/N > 10 for reliable RM and polarization measurements, this 10% level effectively defines a practical detection threshold. The absence of $\sigma_{\rm RM}$ values larger than $\sim$7 rad m^{-2} is therefore plausibly attributable to this same selection effect.

The KDE for the repeating population shows a peak at 1.3 rad m^{-2}. As discussed above, we caution that this peak may be subject to selection bias, since FRBs with larger $\sigma_{\rm RM}$ may not have sufficiently high polarization S/N for reliable measurements. There is also a secondary bump at $\sigma_{\rm RM} \lesssim 0.5$ rad m^{-2}, which may indicate that some repeating FRBs reside in a less complex magneto-ionic environment—a population also identified by Ref. [6]. This is noteworthy given that, while a large proportion of repeating FRBs exhibit RM variations exceeding 50 rad m^{-2}, others exhibit only marginal intrinsic RM variations. Together with previously reported sources, the two FRBs with the largest $\sigma_{\rm RM}$ are FRB 20121102A (30.9 ± 0.4 rad m^{-2}) and FRB 20190520B (218 ± 10.2 rad m^{-2}) [18]. The broad range of $\sigma_{\rm RM}$ values suggests that repeating FRBs may be at different evolutionary stages [18,35] or may even have distinct physical origins.

3.2. Non-Repeating FRBs

Following the method outlined in Section 2, we perform a Bayesian model comparison among all four spectro-polarimetric models for the 70 non-repeating FRBs in our sample. For the 17 sources for which the oscillation model is strongly preferred ($\Delta \log_{10} E \geq 10$), passes the PPC diagnostic, satisfies the amplitude significance criterion ($A/\sigma_A > 7$), and is confirmed by visual inspection, we list the best-fit parameters in Supplementary Table S2 and display the corresponding fits in Supplementary Figure S1. Nevertheless, in the absence of any published reports of systematic instrumental effects in CHIME data, we are presently unable to distinguish between Faraday conversion, instrumental contamination, and other scenarios. Accordingly, we defer a deeper physical interpretation of the oscillating sources to future investigations. For the remaining 53 bursts, the Bayesian comparison among the constant, Burn, and modified Burn models yields 35 sources best described by the constant model, 8 by the Burn model, and 6 by the modified Burn model. The distribution of best-fit models across the full sample is shown in Figure 3e. Supplementary Figure S2 presents the fits of these three models for each burst, and Supplementary Table S3 provides the detailed Bayesian evidence comparison. Representative examples of each successfully fitted category (constant, Burn, modified Burn, and oscillation) are shown in Figure 3. Four bursts could not be adequately fitted by any of the four models; these are shown in Supplementary Figure S3.

About half of the non-repeating bursts are best described by the constant model. This may be due to CHIME's limited bandwidth, which hinders the detection of linear polarization variations across its frequency range. Alternatively, the potential $\sigma_{\rm RM}$ may be too small to produce significant changes within the CHIME band. For instance, for $\sigma_{\rm RM} \lesssim 0.4$ rad m^{-2}, the polarization fraction drops from ∼99% at 800 MHz to ∼89% at 400 MHz (assuming 100% intrinsic linear polarization), a decrease of less than 10%. Given that CHIME-detected FRBs typically have relatively low S/N and we adopt a sub-band S/N threshold of 5, our models are insensitive to non-repeating FRBs with $\sigma_{\rm RM} \lesssim 0.4$ rad m^{-2}. Indeed, 14 (20%) of these bursts are best described by the Burn or modified Burn model, with corresponding $\sigma_{\rm RM}$ values ranging from 0.5 to 1.9 rad m^{-2}. This absence of population-wide frequency-dependent depolarization is consistent with Pandhi et al. [23] (hereafter P24), who similarly found no evidence for it. However, despite using the same underlying CHIME/FRB baseband data, P24 did not identify the same Burn-type depolarized FRBs that we report. This discrepancy likely arises from differing methods and thresholds. Specifically, P24 defined a depolarization ratio $f_{\rm depol} = (L/I)_{500}/(L/I)_{700}$, comparing the band-averaged linear polarization fraction between the 400–600 MHz and 600–800 MHz sub-bands of broadband FRBs, whereas we perform direct model fitting to the frequency dependence of L/I. The apparent discrepancy may also be exacerbated by the higher detection threshold adopted in P24; for instance, some FRBs below the $f_{\rm depol} = 1$ dashed

line in their Figure 11 could exhibit depolarization, particularly those approaching the dash-dotted curve predicted by the $\sigma_{\rm RM}$ model. Nevertheless, P24 did not classify any of these FRBs as depolarized. No cases with $\sigma_{\rm RM} \leq 0.4$ rad m^{-2} are found, likely due to the limitations of the data and our modeling approach. We note that none of these sources exhibit significant depolarization with $\sigma_{\rm RM} \gtrsim 5$ rad m^{-2}.

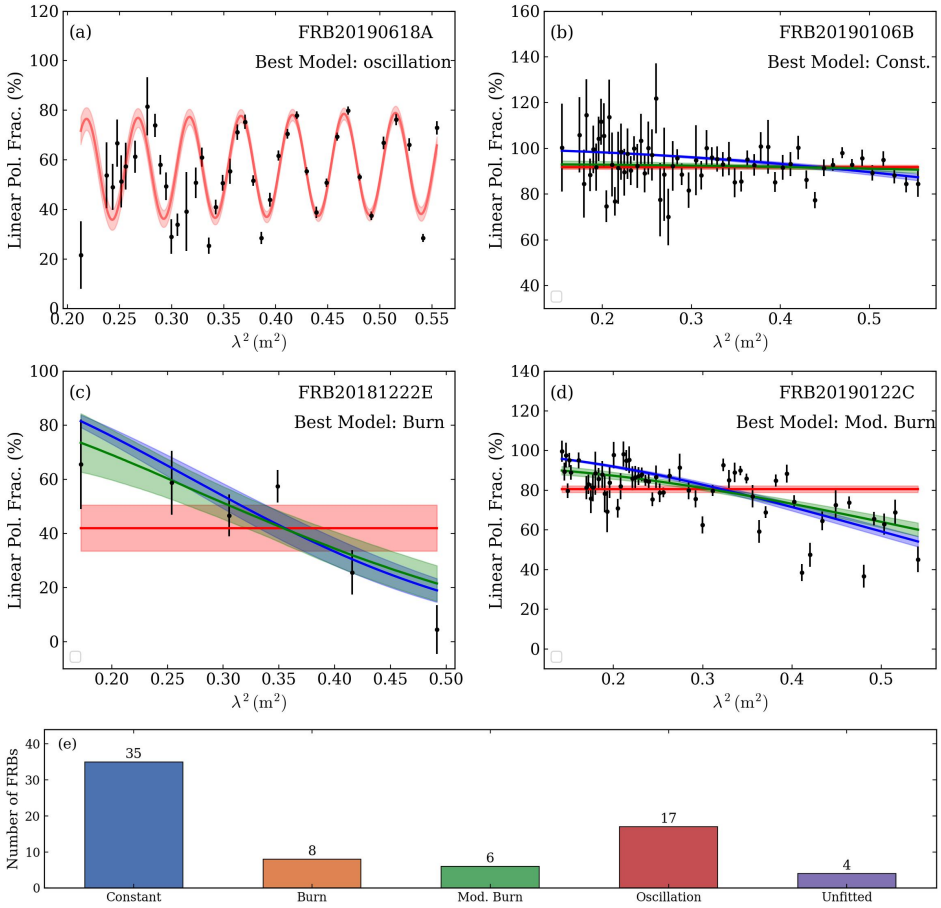


Figure 3. Fractional linear polarization vs. wavelength-squared for four representative non-repeating FRBs, illustrating different best-fitting models: oscillation (**a**), constant (**b**), Burn (**c**), and modified Burn (**d**). Black points with error bars show the data; shaded regions indicate 1σ confidence intervals. Oscillation fit is shown in red in panel (**a**); for other panels, red, blue, and green curves represent Const., Burn, and Mod. Burn models, respectively. The preferred model for each burst is indicated. Panel (**e**) shows the model distribution across the 70 non-repeating FRB sample.

4. Conclusions

We have performed a systematic spectro-polarimetric analysis of 28 repeating and 70 non-repeating fast radio bursts detected by CHIME. For the repeating population, we measured the RM scatter parameter $\sigma_{\rm RM}$ for each source, expanding the known sample from 14 to 36 sources (an increase by a factor of 2.6) compared to previous studies. The KDE of $\sigma_{\rm RM}$ peaks at 1.3 rad m^{-2}, and approximately 70% of the repeaters exhibit $\sigma_{\rm RM} \gtrsim 1$ rad m^{-2}, suggesting that the majority reside in complex magneto-ionic environments. However, we find no repeater with $\sigma_{\rm RM} > 10$ rad m^{-2}; this absence is not a physical upper limit but rather a selection bias inherent to the CHIME band. At 800 MHz, a $\sigma_{\rm RM}$ of 7.6 rad m^{-2} already suppresses the linear polarization fraction to $\sim$10%, below the typical detection threshold given the moderate S/N of the sample. Consequently, the most extreme magneto-ionic environments—if they exist—would remain largely invisible to current polarization-selected surveys, and the true distribution of $\sigma_{\rm RM}$ among repeaters may be significantly

broader than observed. There is also a secondary bump at $\sigma_{\rm RM} \lesssim 0.5$ rad m^{-2}, which may indicate that some repeating FRBs reside in a less magneto-ionic environment. Combined with previously published results, especially from high-frequency observations, the broad range of $\sigma_{\rm RM}$ values suggests that repeating FRBs may be at different evolutionary stages or may even have distinct physical origins.

For the non-repeating FRBs, we characterized their spectro-polarimetric properties by comparing four models: constant, Burn, modified Burn, and oscillation. No significant Burn-type depolarization with $\sigma_{\rm RM} \gtrsim 5$ rad m^{-2} is detected across the sample; in particular, half of the bursts are best described by a constant polarization fraction. Among the remaining sources, 8 favor the standard Burn model, 6 favor the modified Burn model, and 17 exhibit coherent oscillatory patterns in polarization fraction. Notably, four bursts could not be adequately fitted by any of the proposed models. For the 14 Burn-like FRBs, the $\sigma_{\rm RM}$ values lie in the range 0.5 to 1.9 rad m^{-2}. No cases with $\sigma_{\rm RM} \leq 0.4$ rad m^{-2} are found, likely due to the limitations of the data and our modeling approach.

Wideband polarimetric observations, or the combination of polarimetric data from widely separated frequency bands, will enable a more comprehensive characterization of the spectro-polarimetric properties of FRBs. For repeating FRBs that are undetectable in polarization with CHIME, we anticipate that polarization measurements at higher radio frequencies will become feasible, potentially even leading to the discovery of new persistent radio sources associated with these repeaters. Meanwhile, for repeaters that show near-100% linear polarization within the CHIME band, observations with Low Frequency Array (LOFAR) or Square Kilometre Array (SKA)-Low could provide precise constraints on $\sigma_{\rm RM}$. Furthermore, wideband coverage will allow us to determine whether the polarization of non-repeating FRBs is indeed frequency-independent. The new facilities currently under construction are also poised to shape the field [36–39]. For example, DSA-2000 (0.7–2 GHz) is expected to detect and localize FRBs at a rate of $\sim 10^4$ yr^{-1} [36]. Collectively, these efforts will significantly deepen our understanding of FRB environments and radiation physics.

Supplementary Materials: The following supporting information can be downloaded at https://www.mdpi.com/article/10.3390/universe12090256/s1: Figure S1: Oscillation model fits for linear and circular polarization fractions vs. wavelength squared for each non-repeating FRB; Figure S2: Model fit results for each non-repeating FRB; Figure S3: Observed linear polarization fraction vs. wavelength-squared for non-repeating FRBs that could not be fitted with the available models; Table S1: Rotation measure scatter ($\sigma_{\rm RM}$) for 28 repeating FRBs; Table S2: Fitting results for the non-repeating FRBs using the oscillation model; Table S3: Bayesian model comparison for non-repeating FRBs.

Author Contributions: Conceptualization, Y.F.; methodology, D.Z., and Y.F.; software, D.Z.; validation, D.Z. and Y.F.; formal analysis, D.Z.; investigation, D.Z. and Y.F.; resources, Y.F.; data curation, D.Z.; writing—original draft preparation, D.Z., Y.F., J.X. and J.F.; writing—review and editing, D.Z., Y.F., J.X., J.F. and C.X.; visualization, D.Z. and C.X.; supervision, Y.F.; project administration, Y.F.; funding acquisition, Y.F. All authors have read and agreed to the published version of the manuscript.

Funding: This work is supported by National Key R&D Program of China No. 2023YFB4503300, and the National Natural Science Foundation of China under grant 12522305.

Data Availability Statement: The original contributions presented in this study are included in the article/Supplementary Materials. Further inquiries can be directed to the corresponding author.

Acknowledgments: We thank the reviewers for their constructive reports.

Conflicts of Interest: The authors declare no conflicts of interest.

Note

[1] https://blinkverse.zero2x.org

References

1. Lorimer, D.R.; Bailes, M.; McLaughlin, M.A.; Narkevic, D.J.; Crawford, F. A Bright Millisecond Radio Burst of Extragalactic Origin. *Science* **2007**, *318*, 777. [CrossRef]
2. Xu, J.; Feng, Y.; Li, D.; Wang, P.; Zhang, Y.; Xie, J.; Chen, H.; Wang, H.; Kang, Z.; Hu, J.; et al. Blinkverse: A Database of Fast Radio Bursts. *Universe* **2023**, *9*, 330. [CrossRef]
3. Xu, J.; Tsai, C.W.; Lake, S.E.; Feng, Y.; Chen, X.L.; Li, D.; Wang, H.; Guo, X.; Hu, J.; Ge, X. Blinkverse 2.0: Updated Host Galaxies for Fast Radio Bursts. *Universe* **2025**, *11*, 206. [CrossRef]
4. Zhang, B. The physics of fast radio bursts. *Rev. Mod. Phys.* **2023**, *95*, 035005. [CrossRef]
5. Yang, Y.P.; Xu, S.; Zhang, B. Faraday rotation measure variations of repeating fast radio burst sources. *Mon. Not. R. Astron. Soc.* **2023**, *520*, 2039–2054. [CrossRef]
6. Feng, Y.; Zhang, Y.K.; Xie, J.; Yang, Y.P.; Qu, Y.; Zhou, D.; Li, D.; Zhang, B.; Zhu, W.; Lu, W.; et al. Multi-year polarimetric monitoring of four CHIME-discovered repeating fast radio bursts with FAST. *Sci. China Phys. Mech. Astron.* **2025**, *68*, 289511. [CrossRef]
7. Michilli, D.; Seymour, A.; Hessels, J.W.T.; Spitler, L.G.; Gajjar, V.; Archibald, A.M.; Bower, G.C.; Chatterjee, S.; Cordes, J.M.; Gourdji, K.; et al. An extreme magneto-ionic environment associated with the fast radio burst source FRB 121102. *Nature* **2018**, *553*, 182–185. [CrossRef]
8. Hilmarsson, G.H.; Michilli, D.; Spitler, L.G.; Wharton, R.S.; Demorest, P.; Desvignes, G.; Gourdji, K.; Hackstein, S.; Hessels, J.W.T.; Nimmo, K.; et al. Rotation Measure Evolution of the Repeating Fast Radio Burst Source FRB 121102. *Astrophys. J. Lett.* **2021**, *908*, L10. [CrossRef]
9. Anna-Thomas, R.; Connor, L.; Dai, S.; Feng, Y.; Burke-Spolaor, S.; Beniamini, P.; Yang, Y.P.; Zhang, Y.K.; Aggarwal, K.; Law, C.J.; et al. Magnetic field reversal in the turbulent environment around a repeating fast radio burst. *Science* **2023**, *380*, 599–603. [CrossRef]
10. Mckinven, R.; Gaensler, B.M.; Michilli, D.; Masui, K.; Kaspi, V.M.; Su, J.; Bhardwaj, M.; Cassanelli, T.; Chawla, P.; Dong, F.A.; et al. Revealing the Dynamic Magnetoionic Environments of Repeating Fast Radio Burst Sources through Multiyear Polarimetric Monitoring with CHIME/FRB. *Astrophys. J.* **2023**, *951*, 82. [CrossRef]
11. Li, Y.; Zhang, S.B.; Yang, Y.P.; Tsai, C.W.; Yang, X.; Law, C.J.; Anna-Thomas, R.; Chen, X.L.; Lee, K.J.; Tang, Z.F.; et al. A sudden change and recovery in the magnetic environment around a repeating fast radio burst. *Science* **2026**, *391*, 280–284. [CrossRef]
12. Piro, A.L.; Gaensler, B.M. The Dispersion and Rotation Measure of Supernova Remnants and Magnetized Stellar Winds: Application to Fast Radio Bursts. *Astrophys. J.* **2018**, *861*, 150. [CrossRef]
13. Margalit, B.; Metzger, B.D. A Concordance Picture of FRB 121102 as a Flaring Magnetar Embedded in a Magnetized Ion-Electron Wind Nebula. *Astrophys. J. Lett.* **2018**, *868*, L4. [CrossRef]
14. Zhao, Z.Y.; Wang, F.Y. FRB 190520B Embedded in a Magnetar Wind Nebula and Supernova Remnant: A Luminous Persistent Radio Source, Decreasing Dispersion Measure, and Large Rotation Measure. *Astrophys. J. Lett.* **2021**, *923*, L17. [CrossRef]
15. Katz, J.I. FRB 190520B—An FRB in a young supernova remnant? *Mon. Not. R. Astron. Soc.* **2022**, *510*, L42–L44. [CrossRef]
16. Wang, F.Y.; Zhang, G.Q.; Dai, Z.G.; Cheng, K.S. Repeating fast radio burst 20201124A originates from a magnetar/Be star binary. *Nat. Commun.* **2022**, *13*, 4382. [CrossRef]
17. Burn, B.J. On the depolarization of discrete radio sources by Faraday dispersion. *Mon. Not. R. Astron. Soc.* **1966**, *133*, 67. [CrossRef]
18. Feng, Y.; Li, D.; Yang, Y.P.; Zhang, Y.; Zhu, W.; Zhang, B.; Lu, W.; Wang, P.; Dai, S.; Lynch, R.S.; et al. Frequency-dependent polarization of repeating fast radio bursts—Implications for their origin. *Science* **2022**, *375*, 1266–1270. [CrossRef]
19. Chatterjee, S.; Law, C.J.; Wharton, R.S.; Burke-Spolaor, S.; Hessels, J.W.T.; Bower, G.C.; Cordes, J.M.; Tendulkar, S.P.; Bassa, C.G.; Demorest, P.; et al. A direct localization of a fast radio burst and its host. *Nature* **2017**, *541*, 58–61. [CrossRef]
20. Niu, C.H.; Aggarwal, K.; Li, D.; Zhang, X.; Chatterjee, S.; Tsai, C.W.; Yu, W.; Law, C.J.; Burke-Spolaor, S.; Cordes, J.M.; et al. A repeating fast radio burst associated with a persistent radio source. *Nature* **2022**, *606*, 873–877. [CrossRef]
21. Uttarkar, P.A.; Shannon, R.M.; Gourdji, K.; Deller, A.T.; Day, C.K.; Bhandari, S. Searching for the spectral depolarization of ASKAP one-off FRB sources. *Mon. Not. R. Astron. Soc.* **2024**, *527*, 4285–4296. [CrossRef]
22. Uttarkar, P.A.; Shannon, R.M.; Gourdji, K.; Deller, A.T.; Dial, T.; Glowacki, M.; Bera, A.; Gordon, A.C.; Ryder, S.D.; Tejos, N.; et al. A depolarization census of ASKAP fast radio bursts. *Mon. Not. R. Astron. Soc.* **2026**, *545*, staf1997. [CrossRef]
23. Pandhi, A.; Pleunis, Z.; Mckinven, R.; Gaensler, B.M.; Su, J.; Ng, C.; Bhardwaj, M.; Brar, C.; Cassanelli, T.; Cook, A.; et al. Polarization Properties of 128 Nonrepeating Fast Radio Bursts from the First CHIME/FRB Baseband Catalog. *Astrophys. J.* **2024**, *968*, 50. [CrossRef]

24. Ng, C.; Pandhi, A.; Mckinven, R.; Curtin, A.P.; Shin, K.; Fonseca, E.; Gaensler, B.M.; Jow, D.L.; Kaspi, V.; Li, D.; et al. Polarization Properties of 28 Repeating Fast Radio Burst Sources with CHIME/FRB. *Astrophys. J.* **2025**, *982*, 154. [CrossRef]
25. Andersen, B.C.; Bandura, K.; Bhardwaj, M.; Boyle, P.J.; Brar, C.; Cassanelli, T.; Chatterjee, S.; Chawla, P.; Cook, A.M.; Curtin, A.P.; et al. [CHIME/FRB Collaboration] CHIME/FRB Discovery of 25 Repeating Fast Radio Burst Sources. *Astrophys. J.* **2023**, *947*, 83. [CrossRef]
26. Mckinven, R.; Michilli, D.; Masui, K.; Cubranic, D.; Gaensler, B.M.; Ng, C.; Bhardwaj, M.; Leung, C.; Boyle, P.J.; Brar, C.; et al. Polarization Pipeline for Fast Radio Bursts Detected by CHIME/FRB. *Astrophys. J.* **2021**, *920*, 138. [CrossRef]
27. Dunning, A.; Bowen, M.; Castillo, S.; Chung, Y.S.; Doherty, P.; George, D.; Hayman, D.B.; Jeganathan, K.; Kanoniuk, H.; Mackay, S.; et al. Design and laboratory testing of the five hundred meter aperture spherical telescope (FAST) 19 beam L-band receiver. In *Proceedings of the 2017 XXXIInd General Assembly and Scientific Symposium of the International Union of Radio Science (URSI GASS)*; IEEE: New York, NY, USA, 2017; p. 62. [CrossRef]
28. Xu, H.; Niu, J.R.; Chen, P.; Lee, K.J.; Zhu, W.W.; Dong, S.; Zhang, B.; Jiang, J.C.; Wang, B.J.; Xu, J.W.; et al. A fast radio burst source at a complex magnetized site in a barred galaxy. *Nature* **2022**, *609*, 685–688. [CrossRef]
29. Wang, W.Y.; Liu, X.; Li, D.; Zhang, B.; Niu, C.H.; Liu, J.; Xu, R.; Zhu, W.; Lee, K. Propagation-induced Frequency-dependent Polarization Properties of Fast Radio Burst. *Astrophys. J.* **2025**, *988*, 164. [CrossRef]
30. Trotta, R. Bayes in the sky: Bayesian inference and model selection in cosmology. *Contemp. Phys.* **2008**, *49*, 71–104. [CrossRef]
31. Jiang, J.C.; Wang, W.Y.; Xu, H.; Xu, J.W.; Zhang, C.F.; Wang, B.J.; Zhou, D.J.; Zhang, Y.K.; Niu, J.R.; Lee, K.J.; et al. FAST Observations of an Extremely Active Episode of FRB 20201124A. III. Polarimetry. *Res. Astron. Astrophys.* **2022**, *22*, 124003. [CrossRef]
32. Zhang, Y.K.; Li, D.; Zhang, B.; Cao, S.; Feng, Y.; Wang, W.Y.; Qu, Y.; Niu, J.R.; Zhu, W.W.; Han, J.L.; et al. FAST Observations of FRB 20220912A: Burst Properties and Polarization Characteristics. *Astrophys. J.* **2023**, *955*, 142. [CrossRef]
33. Xie, J.T.; Feng, Y.; Li, D.; Zhang, Y.K.; Zhou, D.K.; Qu, Y.; Cui, X.H.; Fang, J.H.; Xu, J.Y.; Miao, C.C.; et al. Polarization Characteristics of the Hyperactive FRB 20240114A. *Astrophys. J. Suppl. Ser.* **2025**, *278*, 49. [CrossRef]
34. Pandhi, A.; Nimmo, K.; Andrew, S.; Brar, C.; Chatterjee, S.; Cook, A.M.; Curtin, A.; Gaensler, B.M.; Gawronski, M.; Hessels, J.; et al. A Steadily Declining Dispersion Measure for the Repeating Fast Radio Burst FRB 20220529A: Evidence for a Fast Radio Burst Engine Embedded in an Expanding Supernova Remnant. *Astrophys. J. Lett.* **2026**, *1000*, L53. [CrossRef]
35. Caleb, M. Unifying repeating fast radio bursts. *Science* **2022**, *375*, 1227–1228. [CrossRef]
36. Hallinan, G.; Ravi, V.; Weinreb, S.; Kocz, J.; Huang, Y.; Woody, D.P.; Lamb, J.; D'Addario, L.; Catha, M.; Law, C.; et al. The DSA-2000—A Radio Survey Camera. In *Proceedings of the Bulletin of the American Astronomical Society*; American Astronomical Society: Washington, DC, USA, 2019; Volume 51, p. 255. [CrossRef]
37. Lin, H.H.; Lin, K.y.; Li, C.T.; Tseng, Y.H.; Jiang, H.; Wang, J.H.; Cheng, J.C.; Pen, U.L.; Chen, M.T.; Chen, P.; et al. BURSTT: Bustling Universe Radio Survey Telescope in Taiwan. *Publ. Astron. Soc. Pac.* **2022**, *134*, 094106. [CrossRef]
38. Luo, R.; Ekers, R.; Hobbs, G.; Dunning, A.; James, C.; Lower, M.; Gupta, V.; Zic, A.; Sokolowski, M.; Phillips, C.; et al. A fast radio burst monitor with a compact all-sky phased array (CASPA). *Publ. Astron. Soc. Aust.* **2024**, *41*, e109. [CrossRef]
39. Connor, L.; Ravi, V.; Sanghavi, P.; Balakrishan, V.; Chung, L.; Daghlian, S.; Dunn, L.; Griffin, A.; Harnach, C.; Hodges, M.; et al. The 256-antenna Coherent All-Sky Monitor. *arXiv* **2026**, arXiv:2604.13903. [CrossRef]

Disclaimer/Publisher's Note: The statements, opinions and data contained in all publications are solely those of the individual author(s) and contributor(s) and not of MDPI and/or the editor(s). MDPI and/or the editor(s) disclaim responsibility for any injury to people or property resulting from any ideas, methods, instructions or products referred to in the content.